Manuscript submitted to *Smart Materials and Structures* 2018

Reconfigurable origami silencers for tunable and programmable sound attenuation

Hongbin Fang[1], Xiang Yu[2] and Li Cheng[1,*]

[1] *Department of Mechanical Engineering, The Hong Kong Polytechnic University, Hung Hom, Kowloon, Hong Kong, China*

[2] *Institute of High Performance Computing, A*STAR, Singapore 138632, Singapore*

Hongbin Fang	Email: hongbin.fang@polyu.edu.hk
Xiang Yu	Email: yuxiang@ihpc.a-star.edu.sg
Li Cheng (* Corresponding author)	Email: li.cheng@polyu.edu.hk

Abstract:

Recent research has discovered that origami-inspired structures possess great versatility in properties and functionalities. In this research, through an integration of origami geometry and duct acoustics, we reveal that the folding-induced shape reconfiguration of a modular-origami silencer could yield great tunability and programmability in sound attenuation. This has been made possible through exploring the kinematics of the folding and the extensibility of the modular origami. Numerical and experimental results indicate that by reconfiguring the silencer via a single degree-of-freedom folding mechanism, the sound attenuation bandwidth can be effectively tuned. Meanwhile, based on a comprehensive understanding on the correlations between the origami geometries and the acoustic characteristics, we exemplify that, by incorporating multiple origami layers in a silencer and by programming their geometries, on-demand sound control can be achieved, e.g., attenuation in the prescribed frequency bands, improved attenuation levels, and broadband attenuations. This proof-of-concept study shows that the proposed folding-based mechanism, along with the modularization design concept, would provide a new way to reconfigure the silencer for acoustic adaptability and inspire new innovation in designing acoustic devices.

Keywords: modular origami, duct acoustics, transmission loss, tunability, programmability

1. Introduction

Acoustic silencers are widely employed in various engineering and architectural applications for noise abatement and control, exemplified by mufflers installed within the exhaust systems of most internal combustion engines, duct silencers in buildings, and firearms sound suppressors, etc. [1]. In these applications, noise would span a wide frequency range, in which the high-frequency components can be easily tackled through dissipations; on the contrary, low-to-mid frequency components are more difficult to handle, which is still a challenging issue. Reactive silencers allow sound attenuation with expansion chambers or resonance tubes through sound reflections due to acoustic impedance mismatches, thus generating acoustically destructive interference with the upstream sound in the designed frequency range [2]. Reactive silencers usually exhibit excellent low-to-mid frequency performance for reducing the amplitude of pure tones or narrowband sound. Despite their obvious advantages of simplicity, the effective frequency range is, however, relatively narrow, and there can exist frequencies at which sound can be transmitted with much lower attenuation. Hence, precise design and optimization of the silencer chambers and resonators are needed to cope with the noise source for significant attenuation [3], which, however, generally requires case-by-case considerations and extensive design efforts. In addition, existing reactive silencers are scarcely capable of altering their performance based on requirements, nor possess adequate versatility to adapt to variable operating conditions. While some efforts have been devoted over the years to tackling these challenges, the implementation is largely limited because the approaches typically require extra electromechanical parts [4] that might complicate the system or smart materials that call for harsh working environment (e.g., high voltages for dielectric elastomer [5,6]). These long-standing challenges in acoustic silencer applications—low-to-mid frequency noise control, lack of structural reconfigurability, acoustic tunability, and design flexibility—motivate people to explore alternative concepts and innovative principles for silencer design.

Recently, origami, the ancient art of paper folding, brings abundant inspirations to diverse engineering fields thanks to its excellent transformability from two-dimensional (2D) crease patterns to three-dimensional (3D) structures. In addition to providing limitless design possibilities [7–9], folding-induced reconfiguration would also impart favorable characteristics to origami-inspired structures and material systems. Some of these newly uncovered properties are missing in conventional bulk materials and engineering structures. Considering that origami folding and the associated properties are entirely determined by geometry that are scale-independent, origami triggers an explosion of innovations in reprogrammable metamaterials [8,10,11], multistable and self-locking morphing systems [12–16],

foldable robots and devices [17–19], and deployable structures [20,21], which span from nanometer [22] to meter levels [23]. In these applications, *folding* offers the long-expected *tunability* and *programmability* to various properties, including stiffness [10,24], Poisson's ratio [8,25], thermal expansion [11], and electromagnetic radiation [26,27].

The folding-induced tunability also starts to receive attentions from the acoustic community, although, the so-called origami acoustics is still in its infancy when compared with other disciplines. Based on Miura-ori and star-shaped origamis, reconfigurable acoustic arrays were designed to reversibly change the wave energy focusing [28,29]. Inspired by origami snapology, a new type of reconfigurable acoustic wave-guide was proposed to achieve very different acoustic responses and wave radiation patterns in a broad frequency range [30]. Although not foldable, origami-based core panels were proved to be effective in insulating low-frequency sound [31]. Origami could also be treated as a platform to guide the reconfiguration of the associated arrays of inclusions via folding, which can be potentially developed into a tunable traffic noise barrier [32,33]. These successful applications of folding algorithms in acoustics suggest that origami might also become a novel and viable tool for designing reconfigurable silencers.

An acoustic silencer is desirable if its sound attenuation performance can be adaptively tuned and on-demand programmed via a simple actuation mechanism. By establishing an analogy between the silencer reconfiguration and origami morphing, new concepts for reconfigurable silencer can be explored to address the deficiencies of traditional, unchangeable silencers via straightforward origami folding techniques. Foreseeable advantages of such a design are multiple. First, origami folding can be employed to reconfigure a duct silencer and thus to alter its sound transmission and attenuation characteristics. Such a reconfiguration process is reversible and requires only one drive because folding of the origami structure is a single degree-of-freedom (DoF) mechanism. Practically, one actuation could significantly simplify the implementation and make it convenient to realize real-time feedback control. Second, origami design holds inherent extensibility provided that the kinematic compatibility is satisfied; this allows customizing or iterating the silencer architecture according to the requirements following a *modularization* concept. Thus, instead of re-designing the structure entirely, the silencer performance can be conveniently programmed by adding or subtracting compatible origami modules, which is a significant advantage in terms of design flexibility.

In this paper, by associating the knowledge obtained from origami science with duct acoustics theory, we explore the on-demand tunability and programmability of sound attenuation realized through

an origami silencer. Focusing on the conceptual design, the flow effect and its analysis are neglected in this study. As a proof-of-concept study, this research aims at revealing the promise of the origami concept in designing and tuning silencers, rather than putting forward a new product and comparing with previously developed products in terms of performance. Nevertheless, the exemplification illustrates that the new origami-based design idea and the folding-based reconfiguration principle would apply effectively to real products and extend well to other sound-blocking devices, such as acoustic meta-surfaces that allow balancing sound insulation and air ventilation functions [34,35].

In the following sections, the origami structure under investigation is first introduced and examined, and the corresponding silencer design is proposed. Numerical results are then reported and discussed to demonstrate the effectiveness of the acoustic tuning via folding, which are verified with experiments based on a proof-of-concept prototype. Following that, comprehensive parameter studies and numerical optimization examples are carried out to uncover the unique programmability of the proposed origami silencers.

2. Modular origami geometry and conceptual design

Considering the special requirements from duct acoustics, a particular origami type known as *modular origami* is considered. Unlike conventional origami structures that are obtained by stacking folded patterns from a single piece of paper, modular origami first folds multiple pieces of papers into a module and then interlocks these modules together into a 3D structure. An example of the modular origami concept is *knotology*, which connects paper-stripe-folded modules into a 3D interlocked assembly [36]. Among boundless knotology designs, transformable knotology structures are of particular interest to researchers because of their high reconfigurability and extensibility, whose values have been proved in developing reconfigurable metamaterials with controllable mechanical and acoustic properties [9,30,37]. As an example, Figure 1(a) shows the photos of a typical knotology structure, a cube assembly, which is able to transform among different configurations.

If treating the cubes and the void as 2D shapes, the cube assembly prototype can be described as a 2D tiling pattern (Figure 1(b)), which consists of four interconnected square ‘tiles’ that surround a ‘void’. Its geometry can be characterized by the edge length a and the folding angle θ of the ‘void’ (Figure 1(b)). Note that the ‘tiles’ are not necessary to be square; rectangle ‘tiles’ (with edge lengths a and b) can still have the same ‘void’ and the same folding kinematics as the square case, provided that the edges shared by the ‘tiles’ and the ‘void’ remain unchanged (Figure 1(c)). This property endows the

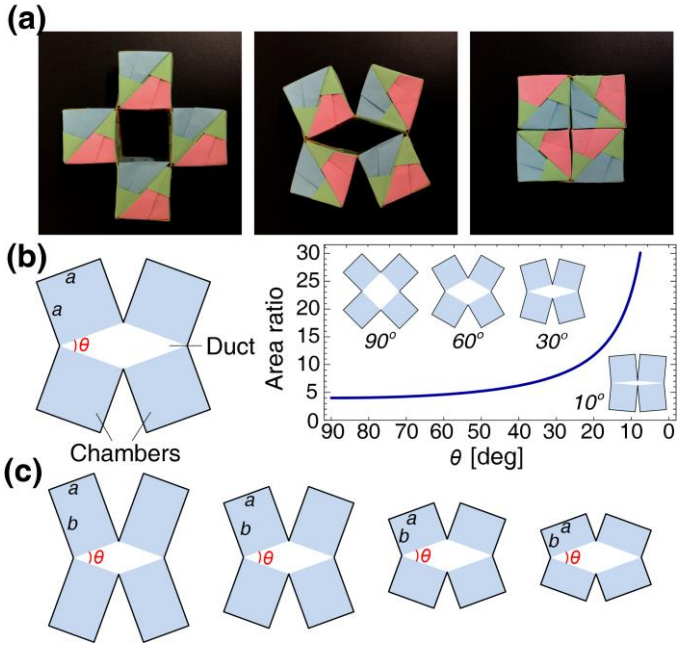

Figure 1. Geometry of a modular origami, a cube assembly, and its transformation. (a) Photos of a paper prototype at three different configurations; (b) the corresponding 2D tiling pattern and the area ratio changes with respect to folding angles; (c) other compatible designs with different rectangle 'tiles'.

modular origami with great extensibility such that layers with different 'tile' geometries can be compatibly connected in series and synchronously reconfigured via folding.

As an example, we examine the transformation of the cube assembly (Figure 1(b)) by characterizing the area ratio between the 'tiles' and the 'void' (i.e., $\gamma = S_{\text{tiles}} / S_{\text{void}} = 4/\sin\theta$). When the origami is folded from $\theta = 90^\circ$ to 0°, the internal 'void' transforms from a square to a rhombus, and finally it closes; correspondingly, the area ratio increases quickly when θ decreases.

Drawing an analogy between the "void" and the acoustic duct, as well as the "tiles" and the acoustic chambers (Figure 1(b)), a reconfigurable origami silencer can be therefore conceived. Considering that the relative size relation between the chambers and the duct plays an important role in determining the sound attenuation performance of silencers [38], and folding just provides a variation mechanism on this relation, we surmise that such an origami silencer could offer good folding-induced tunability on sound attenuation. To test the idea, a single-layer origami silencer and the attached duct are modeled (Figure 2(a)). The layer possesses four identical chambers, each being a cuboid with edge lengths a, b, and w. The associated duct's cross-section shares the same geometry and transformation as the rhombus 'void' (with edge length a). Moreover, with the abovementioned extensibility, a multi-layer origami silencer can also be constructed. Figure 2(b) shows a 4-layer silencer, where the layers are

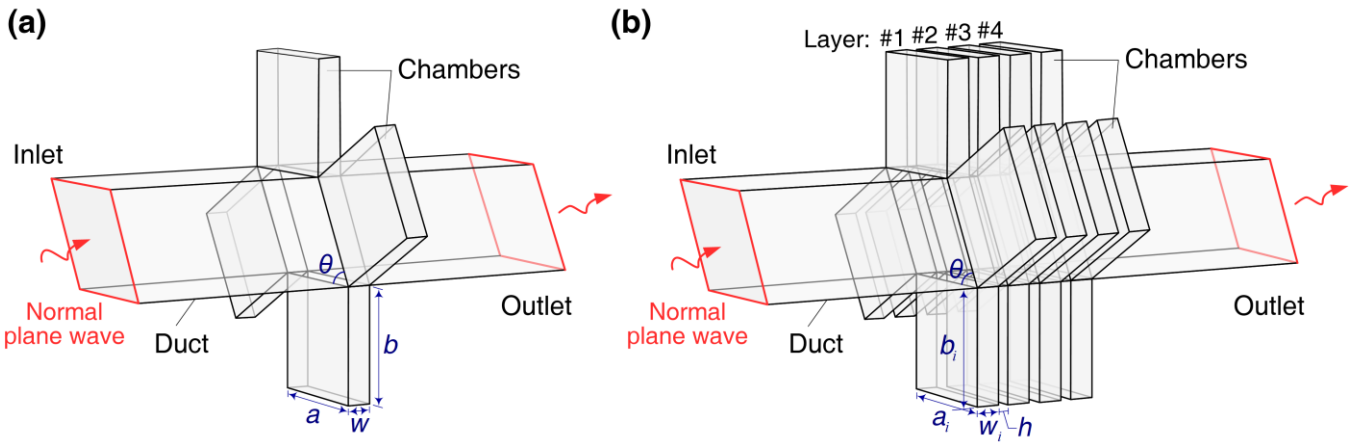

Figure 2. Conceptual designs of (a) a single-layer origami silencer and (b) 4-layer origami silencer. Chambers within each layer share the same dimensions.

arranged with a constant interval h; each chamber in layer i is a cuboid with edge lengths a_i, b_i, and w_i, $i=1,2,3,4$. Note that the edges shared with the void in all layers should have the same length (i.e., $a_i = a,\ i=1,2,3,4$) to guarantee the kinematic compatibility.

3. Folding-induced acoustic tunability

Based on the proposed conceptual design, this section studies how folding-induced silencer reconfiguration would alter the sound attenuation performance. As an example, two simple configurations are considered: a single-layer silencer with $a=b=0.1$ m and $w=0.02$ m; and a 4-layer silencer containing four identical layers with $a_i=b_i=0.1$ m, $w_i=0.02$ m and $h=0.005$ m ($i=1,2,3,4$).

3.1. Simulation setup

Due to the complex geometric layout of the origami silencers, finite element (FE) models (Figure 2) are built using the commercial multiphysics software COMSOL, where the acoustic domain is discretized into nodal coordinates, with the maximum distance of 0.019 m between the nodes. With harmonic excitations, the governing Helmholtz equation for the acoustic pressure p can be expressed as

$$\nabla^2 p + k^2 p = 0, \tag{1}$$

where k is the wave number. All the wall structures in the model are assumed to be acoustically rigid. A plane wave excitation is imposed at the inlet of the duct, and anechoic termination is assumed at the outlet. Here, acoustically rigid means a total and perfect acoustic wave reflection at the boundaries without any energy loss; and anechoic termination corresponds to a non-reflection boundary condition.

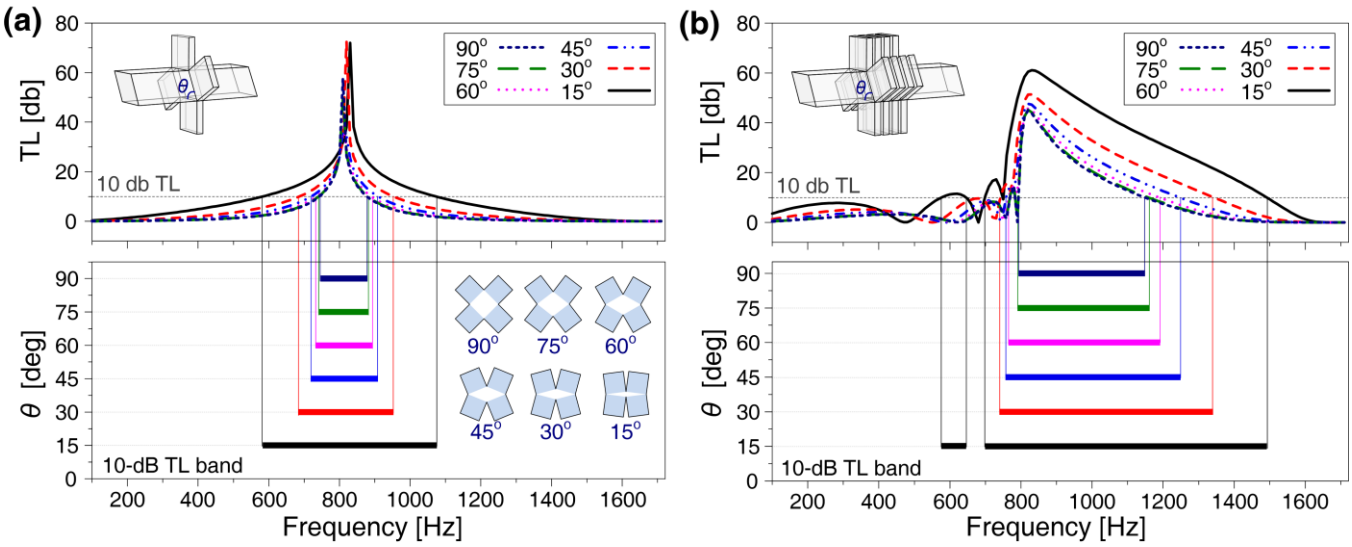

Figure 3. Transmission loss curves (top) and the 10-dB TL bands (bottom) of (a) a single-layer origami silencer and (b) 4-layer origami silencer at six folding configurations. In (a), the 2D tiling patterns at different configurations are given.

The transmission loss (TL), defined as the difference between the power of the incident wave at the inlet (Π_{in}) and the that of the transmitted wave into an anechoic termination (Π_{out}), is evaluated here,

$$\text{TL} = 10\log_{10}\left(\Pi_{\text{in}} / \Pi_{\text{out}}\right). \tag{2}$$

To show the folding effect, both the single-layer and 4-layer silencers are examined for six different folding configurations ($\theta = 15^\circ$, 30°, 45°, 60°, 75°, and 90°). Focusing on the control of the low-to-mid frequency noise, the excitation frequency is set between 100 Hz and 1700 Hz, which is below the cut-off frequency of the rectangle duct with a $100\,\text{mm}\times 100\,\text{mm}$ cross-section (i.e., $a = 0.1\,\text{m}$ so that $f_{\text{cut-off}} = c/2a \approx 1700$ Hz, corresponding to a wavelength of 0.2 m that is much larger than the cross-sectional dimension of the duct) . In such a scenario, higher order modes will not emerge, and the sound wave can be treated as a plane wave.

3.2. Tunable broadband sound attenuation

We first study a single-layer origami silencer. In Figure 3(a), the TL curves corresponding to the six folding configurations are presented. Note that all TL curves peak around 820 Hz and shift little with respect to the folding angle. Around this peak frequency, Helmholtz resonance occurs such that the sound wave is prevented from being transmitted in the downstream direction, analogous to a short circuit owing to the impedance mismatch. However, the breadth of the curves changes significantly due to the folding. For analysis purpose, the so-called effective sound attenuation is set at a 90% reduction in

the sound power (i.e., TL greater than 10 dB). Hence for each configuration, the effective frequency band can be obtained and is plotted in the bottom panel of Figure 3(a). It reveals that decreasing the folding angle θ could significantly expand the effective bandwidth, from 134 Hz at $\theta = 90^\circ$ to 490 Hz at $\theta = 15^\circ$, which is a more than 2 times increase.

Note that based on the reactive mechanism, the frequency range over which the single-layer silencer is effective is relatively narrow. However, previous research indicated that cascading multiple elements such as Helmholtz resonators or expansion chambers into a series can improve the bandwidth of the sound attenuation [39,40], resulting in a TL curve which can be roughly considered as a superposition of the respective TL curve of each element with some variations due to the acoustic coupling among them. Here we show that the modular origami is just a good platform to cascade multiple "elements" without compromising the simplicity of reconfiguration. In the present case, the so-called element is obviously the combination of one origami layer and the gap between the two layers. Instead of independently controlling each individual layer, multiple layers can still be folded as a whole via a single DoF mechanism that requires only one drive. Figure 3(b) shows the TL curves of this 4-layer silencer for the same six configurations. Similarly, 10-dB TL is selected as the threshold of effective sound reduction, and the corresponding effective frequency bands are plotted in the bottom panel. Comparing with the single-layer situation, while the peak TL frequency (i.e., the Helmholtz resonance frequency) changes little with the increase of the layers, the effective bandwidth receives a remarkable improvement. When $\theta = 90^\circ$, the bandwidth expands from 134 Hz to 356 Hz, which is a more than 1.5 times increase with respect to its single-layer counterpart; with $\theta = 15^\circ$, the bandwidth enlarges from 490 Hz to 812 Hz, which is another increase by 65%.

It is worth noting that setting rational gaps between cascaded chambers (i.e., h in Figure 2(b)) is important for improving the silencer's performance [39]. Such gaps introduce sudden changes or discontinuities in the cross-section of the duct. By the same token, this creates a discontinuity in the acoustic impedance in the duct to increase the sound reflections, which subsequently improves the sound attenuation performance. Note that studying the effects of the gap and its design is out of this paper's scope; in the following simulations and experiments, a rational value ($h = 0.005$ m) is used.

The above two examples demonstrate the capability of the reconfigurable origami silencer in tuning the sound attenuation performance. Without replacing chambers, the silencer could effectively reconfigure its shape via folding and reversibly tune the attenuation bandwidth (10-dB TL). Meanwhile, by making use of the modular origami's extensibility and taking advantage of the superposition effect

the attenuation bandwidth can be further enlarged by cascading multiple identical layers. Such a feature would be especially appealing in controlling noise that is broadband but still has a dominant frequency component.

4. Experimental verification

This section reports experimental efforts to ascertain the aforementioned folding-induced acoustic tunability. Specifically, a 4-layer origami silencer prototype is designed and fabricated, based on which the TL at different folding angles are measured to qualitatively verify the numerical predictions.

4.1. Experimental prototype

Figure 4(a) shows the CAD design of a 4-layer origami silencer. Each layer possesses four identical cubic chambers with an inner dimension $0.12\ \mathrm{m}\times 0.08\ \mathrm{m}\times 0.02\ \mathrm{m}$. Adjacent layers are separated by partitions with a thickness 0.005 m. A diamond-shape duct with a side length $0.1\ \mathrm{m}$ crosses over the four layers. We use 10mm-thick acrylic plates to fabricate the prototype. To ensure foldability, flexible hinges are installed between duct walls. To prevent sound leakage, adhesive-back ultrahigh molecular weight (UHMW) polyethylene films are pasted at the connections between acrylic plates, and glues are applied at the hinges and screws. Figure 4(b) displays the photo of the final prototype, with the close-up picture showing the places where the films and the glues are applied. Note that the prototype's dimensions are slightly different from the simulation model given in Figure 2(b). This is to ensure the

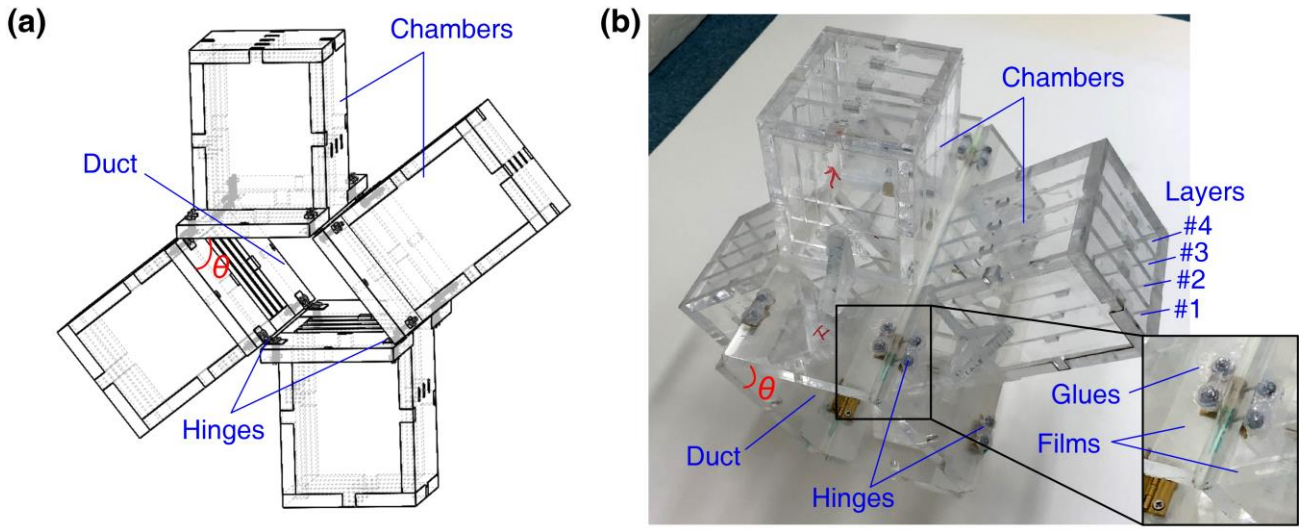

Figure 4. (a) CAD design and (b) prototype of a 4-layer origami silencer. The close-up picture shows the places where the adhesive-back films and glues are applied.

full foldability of the prototype with non-negligible wall thickness, i.e., the prototype is able to achieve all folding configurations from $\theta = 0^\circ$ to 90°.

4.2. Experimental setup

The acoustic measurement is conducted in a rectangle duct with a cross-section of $100\ \text{mm} \times 100\ \text{mm}$. Figure 5 shows the whole measurement system, in which the origami silencer prototype is installed at the center of the duct working section. Here, for the purpose of qualitatively verifying the folding effect, adapters are 3D-printed to connect the main duct (square cross-section) with the duct on the prototype for different configurations (diamond-shape cross-section), as shown in the insect of Figure 5. Two pairs of B&K condenser-type microphones (type 4187, referred as Mic. 1 to Mic. 4) are installed, flush with the duct inner walls. The microphones are supported by a B&K conditioning amplifier (type 2691), and the signals are acquired through an A/D conversion card (NI, PCI-4452). The input signals (sine signals) from the D/A converter (NI, PCI-M10-16E-1) feed a loudspeaker via an audio power amplifier (Lab Gruppen, LAB 300). Both the A/D and D/A processes are controlled by a LabView program, which is made to run through a series of testing frequencies from 100 Hz to 1700 Hz with a step of 10 Hz.

As a widely accepted approach, the two-load method [41–44] is used to measure the TL of the origami silencer, which does not call for a complete absorption anechoic end. Rather, the normal rigid and acoustic foam end can be used for the TL measurement. To make the paper compact, details on how to measure the TL and the related analytical expressions are omitted. In the test, the duration of the measurement at each frequency is long enough (> 1 second) to allow the averaging of the signals and to ensure a steady-state before moving to the next frequency. The acquisition rate is set as $1024 \times f/10$ Hz, which automatically adjusts as the frequency varies.

4.3. Experimental results and discussions

The TL of the origami silencer prototype at three folding configurations ($\theta = 90^\circ$, 60°, and 30°) are measured and plotted in Figure 6(a). For comparison purpose, FE simulation is also performed on the experimental model, and the obtained TL curves are given in Figure 6(b). To show the effectiveness of the origami silencer, the 10-dB TL bands are displayed in Figure 6(c). Qualitatively, good acoustic attenuation performance of the origami silencer is observed in experiments, and the folding-induced acoustic tunability is well confirmed. Figure 6 indicates that folding could effectively tune the attenuation bandwidth: by folding the prototype from $\theta = 90^\circ$ to 60°, and to 30°, the 10-dB TL band enlarges from 350 Hz to 410 Hz, and to 550 Hz.

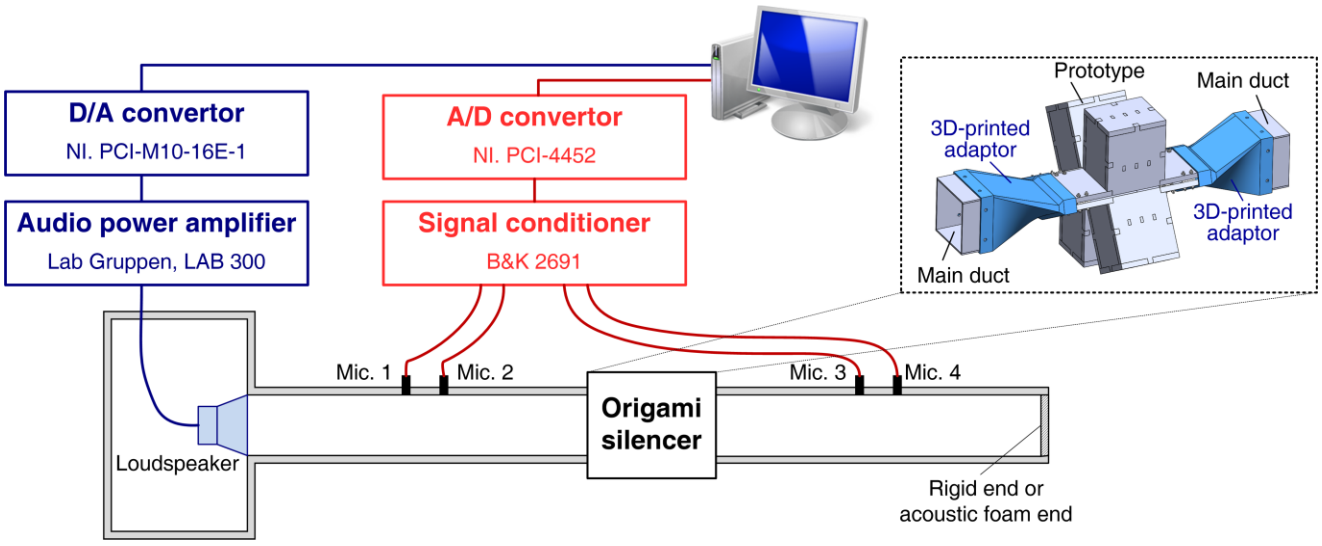

Figure 5. The duct acoustic measurement system. The inset shows the connection between the main duct and the prototype with 3D-printed adaptors.

Quantitatively, there are some discrepancies between the experiment and simulation TL curves, and particularly, the experimental 10-dB TL bands are wider than the simulation ones. This can be attributed to a few plausible reasons. First, the duct cross-section experiences sudden changes at the connections between the main duct and the prototype. Although a streamline design is adopted for the 3D-printed adaptors, due to the limited length of the adaptors, plane wave propagation cannot be fully ensured at the inlet and outlet of the silencer, which may induce additional reflections of the sound wave and affect the TL results. Second, the 3D-printed adaptors and the UHMW polyethylene films are not ideally acoustically rigid because they are much thinner than the walls of the prototype, which may absorb some energy and therefore enhance the attenuation performance. Nevertheless, the prototype and tests are still effective in validating the folding-induced variation trend in the TL of the origami silencer predicted by the simulations.

Note that in the experiments, we manually fold the prototype to the prescribed configurations. In practice, this can be done through any actuation mechanisms that are able to achieve rotations, such as conventional servo-motors or active materials (e.g., shape memory alloys). By adopting specific actuators, careful designs are necessary to keep the full foldability and to ensure the compatibility and compactness of the system.

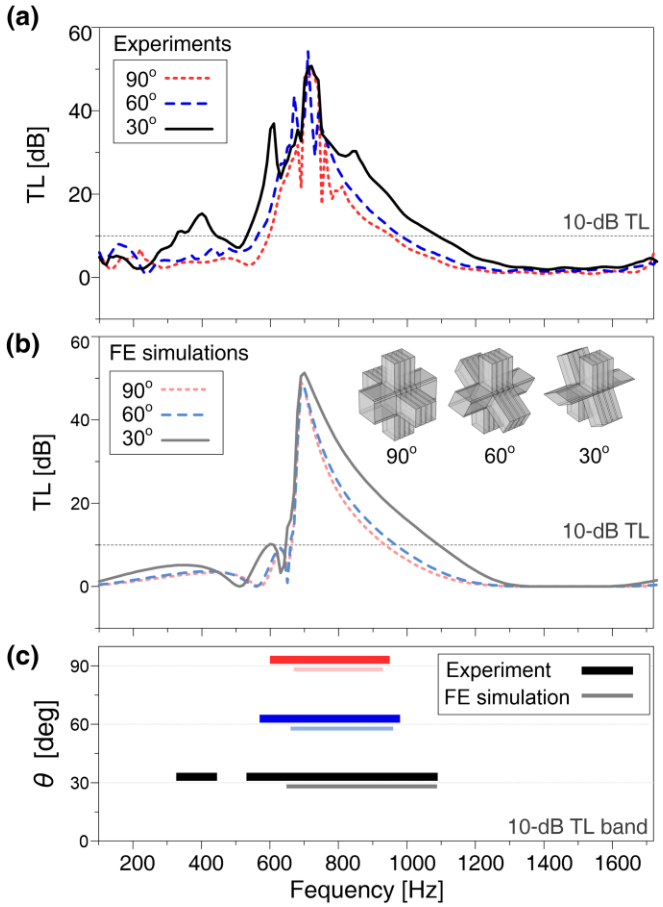

Figure 6. Experiment and simulation results of the origami silencer prototype. From (a) to (c) shows the experiment TL curves, simulation TL curves, and the 10-dB TL bands, respectively. Three configurations are examined in both experiments and simulations: $\theta = 90^\circ$, 60°, and 30°.

5. Acoustic programmability

The results in Figure 3(b) and Figure 6 suggest that multiple chamber layers can facilitate broadband sound attenuation. This motivates a further exploration on the possibilities of cascading different compatible layers in an origami silencer to achieve on-demand sound attenuation. Thus, rather than completely re-designing the silencer, we show in this section that by making use of modular origami's extensibility, the attenuation bandwidth and attenuation level can be adjusted via programming the constituent chamber layers. Such an acoustic programmability is a unique feature of the modular-origami-based design.

5.1. Acoustic characterization and optimization on modular origami layers

As mentioned in Section 2, the origami kinematic compatibility can be ensured, provided that the internal 'voids' of different layers are consistent, i.e., they share the same edge length a (here $a = 0.1$ m). The chamber height b and the chamber width w are parameters to be designed. Practically, we constrain the parameters b and w as follows to prevent oversize or undersize design that may be difficult to achieve in practice:

$$0.05 \le b \le 0.175 \text{ (m)}, \ 0.01 \le w \le 0.08 \text{ (m)}. \tag{3}$$

To effectively program the constituent layers, a comprehensive understanding of different layers' acoustic characteristics is essential and important. To this end, considering each layer as an individual single-layer silencer, we numerically examine their sound attenuation performance based on FEM in COMSOL, with the same setup shown in Figure 2(a).

Figure 7 shows the effect of changing layer geometries on the sound attenuation performance, with $b \in [0.05,\ 0.075,\ 0.1,\ 0.125,\ 0.15,\ 0.175]$ (m) and $w \in [0.01,\ 0.02,\ 0.03,\ 0.04,\ 0.05,\ 0.06,\ 0.07,\ 0.08]$ (m). Three folding configurations with $\theta = 90^\circ$, 45°, and 15° are studied. Similarly, only the frequency range $[100,\ 1700]$ (Hz) below the cut-off frequency is focused. The acoustic 10dB–TL stopbands and the TL peaks are denoted with shaded areas and dashed curves, respectively. Comparing the silencers with the same geometry but different folding angles, the folding-induced bandwidth tuning is observed again. More importantly, Figure 7 reveals that with a relatively large b, there exist two 10-dB TL bands below the cut-off frequency where the silencer could achieve effective sound attenuation. Decreasing the value of b significantly shifts both TL peaks toward higher frequencies as well as enlarges their effective bandwidths. However, when the value of b is excessively small, the second band, and even the first band may exceed the cut-off frequency, which is beyond our scope of interest. On the other hand, enlarging w could also effectively amplify the 10dB-TL stopbands as well as raise the TL peaks, although the peak-raise effect is not as significant as reducing b. These results confirm that the TL peak frequency and effective bandwidth are closely related to different geometrical parameters, which are consistent with the open literature [45].

Overall, by varying the geometry parameters with constraints (3), the TL peaks and 10-dB TL bands are adjustable over a large frequency interval. For example, with $\theta = 15^\circ$, the first TL peaks can vary between 480 Hz (achieved at $b = 0.175$ m, $w = 0.01$m) and 1690 Hz (achieved at $b = 0.05$ m, $w = 0.08$m); and the effective first TL bandwidth can change from 153 Hz (achieved at $b = 0.175$ m, $w = 0.01$m) to 1359 Hz (achieved at $b = 0.075$ m, $w = 0.08$m). In addition to this, Figure 7 also allows

us to quantitatively evaluate the single layer's attenuation performance within a targeted frequency region, based on which, an optimal design can be obtained. Note that optimization on particular silencers has been attempted by many researchers, with major attentions lying on globally optimizing the silencer shapes [46], optimizing the layout of internal partitions [47], and optimization techniques [48]. In these studies, the averaged TL has always been employed as the objective function due to its easy implementation. Here, we also examine the averaged TL of a specific layer design x, which is defined as follows:

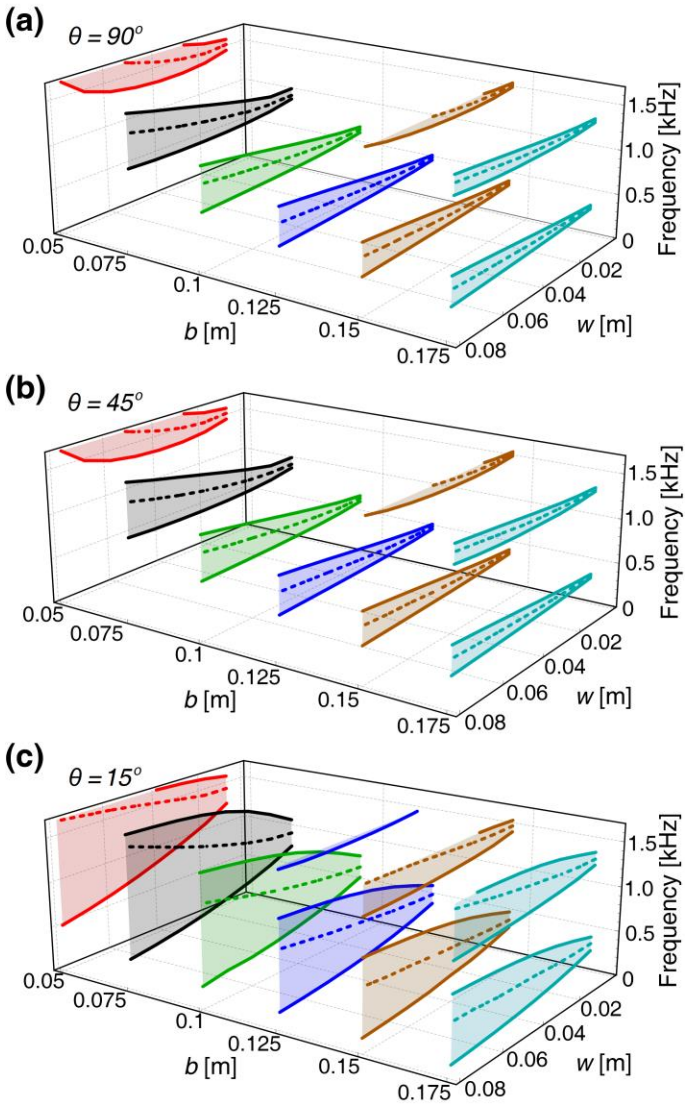

Figure 7. Acoustic characterization of individual origami chamber layer at different folding configurations (a) $\theta = 90^{\circ}$, (b) $\theta = 45^{\circ}$, (a) $\theta = 15^{\circ}$. The solid curves denote the upper and lower boundaries of the 10dB-TL stopbands (shaded areas), and the dashed curves denote the TL peaks.

$$F(x)=\overline{\mathrm{TL}(\Delta f)}=\frac{1}{f_u-f_l}\int_{f_l}^{f_u}W(f)\cdot\mathrm{TL}(f)\mathrm{d}f=\frac{1}{N}\sum_{i=1}^{N}W_i\cdot\mathrm{TL}_i, \tag{4}$$

where f_l and f_u denote the lower and upper bounds of the target frequency band; i denotes the discrete frequency points used in numerical simulations, with a total number N. Here we assume all frequencies have the same weighting $W_i\equiv 1$. Hence, the optimization can be formulated as

$$\max_x\ F(x)\quad\text{for}\quad x=\{x_1,x_2,...\}, \tag{5}$$

where x_1, x_2,... are the design candidates used in simulations that satisfy constraints.

In this paper, based on limited sweeps of the design spaces (b and w), the maximum average TL is numerically determined to exemplify the potential benefit that a more rigorous optimization could achieve. Although such process is not sufficiently rigorous in terms of optimization, the optimal layer geometries can still be determined within the prescribed domains of b and w. Such procedure has also been adopted in other sub-chamber optimization studies [38].

As an example, we select [1000, 1200] Hz as the target frequency band and discretely calculate the averaged TL for two configurations with $\theta=15^\circ$ and $\theta=90^\circ$, respectively. Figure 8 shows the distribution of the averaged TL defined in Eq. (4) with respect to b and w. The design domain is constrained by Eq. (3), and the frequency step is set as 10 Hz. With $\theta=15^\circ$ and $\theta=90^\circ$, the optimal geometric parameters converge to ($b=0.1$ m, $w=0.07$ m), and ($b=0.075$ m, $w=0.05$ m), respectively. This indicates that with the same targeted frequency band, the optimal layer designs for different folding configurations may be different, which calls for special attention in applications. It is also worth pointing out that if the numerical simulations were more comprehensive, i.e., with smaller steps of b and w, the optimization results would have been even finer.

Figure 9 displays another set of four numerical optimization cases with targeted frequency bands $500-600$ Hz, $900-1000$ Hz, $1100-1400$ Hz, and $300-1600$ Hz. The folding configuration is fixed at $\theta=15^\circ$. The optimal designs for these four cases are also obtained by numerical optimizations with the objective function given in Eq. (4). They converge to $b=0.175$ m and $w=0.07$ m, $b=0.1$ m and $w=0.05$ m, $b=0.075$ m and $w=0.05$ m, and $b=0.1$ m and $w=0.08$ m, respectively.

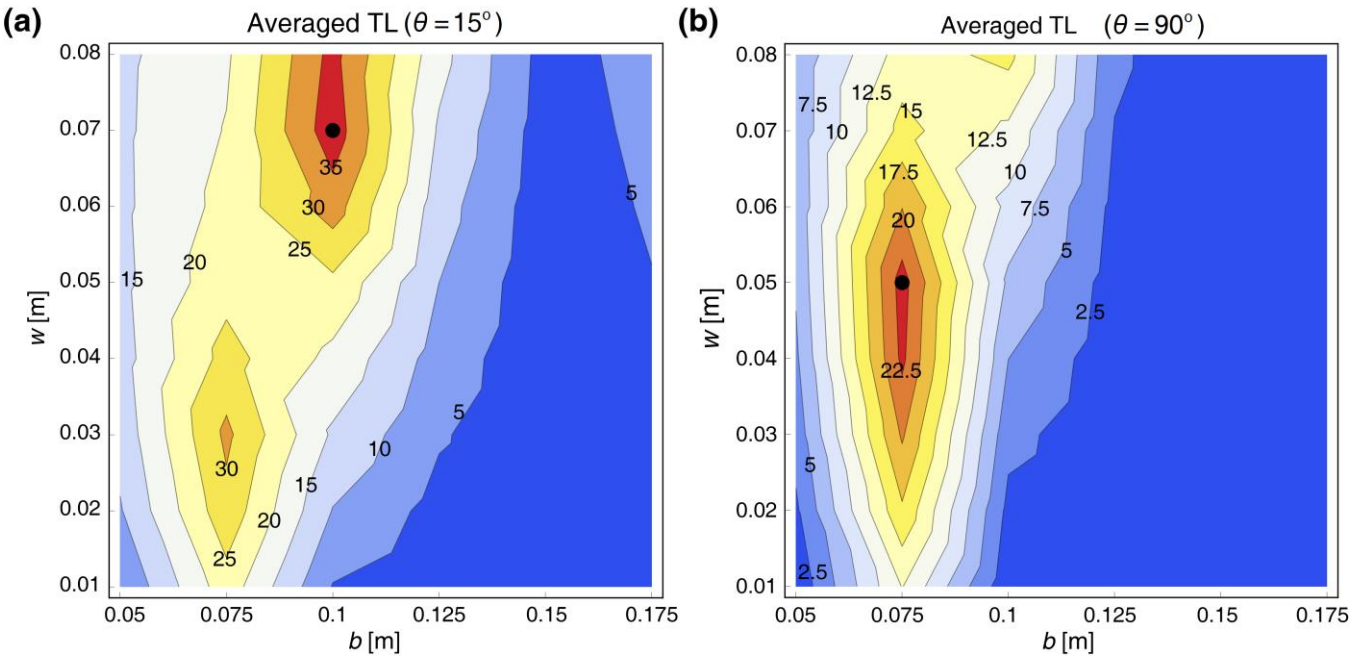

Figure 8. Distributions of the averaged TL with respect to the geometric parameters b and w (the length of the other chamber edge remains constant as $a = 0.1$ m). Two folding configurations are examined: (a) $\theta = 15^\circ$, (b) $\theta = 90^\circ$. The solid dots denote the optimal layer designs corresponding to the maximum averaged TL.

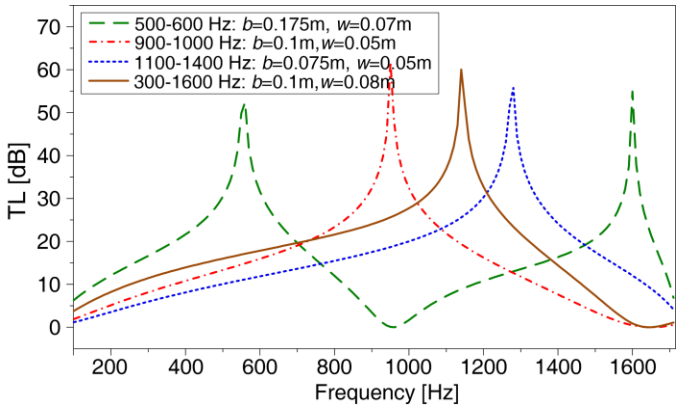

Figure 9. Optimized TL curves for four targeted frequency bands. The optimal geometric parameters are provided.

5.2. Programmability based on combined effect of cascading multiple optimized layers

In addition to finding the optimal geometries of a single-layer silencer, the optimized layers can be further cascaded into a multi-layer silencer for improved acoustic performance, similar as the sub-chamber optimization technique [38]. The great extensibility of the modular origami makes it possible to employ a *modularization* concept to program the constituent layers to meet specific sound attenuation

requirements. Without 'globally' re-designing or re-fabricating the silencer, required sound attenuations can be achieved in a relatively easy way by programming and replacing the constituent functional layers. These layers can be prepared in advance as basic building modules.

With a comprehensive understanding on the single-layer acoustic characteristics, three examples are studied in this subsection to validate the programmability and modularization design philosophy. The total width of the multi-layer silencer is constrained by $\sum_i w_i = 0.08$ m. In the first example (Figure 10(a)), we aim at an effective sound attenuation within the frequency region [600, 1100] Hz; in the second example (Figure 10(b)), the targeted frequency band is set at [1000, 1500] Hz; in the third example (Figure 11), we look for a broadband sound attenuation.

In the first example, four frequency sub-intervals are focused for programming the constituent layers. Their ranges are 500-600 Hz, 600-700 Hz, 700-900 Hz, and 900-1100 Hz, respectively. For the configuration with $\theta = 15^\circ$, the lowest band can be achieved by $b = 0.15$ m and $w = 0.02$ m, which corresponds to a TL peak at 560 Hz; the 600-700 Hz band is obtained by $b = 0.1$ m and $w = 0.02$ m, corresponding to a TL peak at 670 Hz; the 700-900 Hz band is realized by $b = 0.125$ m and $w = 0.02$ m, giving rise to a TL peak at 830 Hz; and the highest band is a result of $b = 0.075$ m and $w = 0.02$ m, with a TL peak at 1080 Hz. When the four constituent layers are cascaded into a four-layer chamber, the required attenuation within 600-1100 Hz is successfully achieved. Even at the most unappealing configuration with $\theta = 90^\circ$, the 10dB-TL band still covers the whole targeted band. For the configuration with $\theta = 15^\circ$, the effective band extends from 500 Hz to 1700 Hz. In addition to the enlarged bandwidth, the attenuation performance within the targeted frequency region is also significantly improved. For the $\theta = 15^\circ$ configuration, the 20dB-TL band also covers the whole targeted frequency band, which indicates a more than 99% reduction of the sound power. With larger θ angles, although the targeted band is not fully covered, 20-dB TL is still achievable in many regions.

The second example further illustrates the programmability and the modularization concept of the modular origami design (Figure 10(b)). By replacing the constituent silencer layers, we successfully achieve sound attenuation at the 1000-1500 Hz band. From $\theta = 90^\circ$ to $\theta = 15^\circ$, the 10-dB TL band covers the whole targeted band for all configurations; moreover, for the $\theta = 15^\circ$ and $\theta = 45^\circ$ configurations, the 20-dB TL band also fully covers the targeted band.

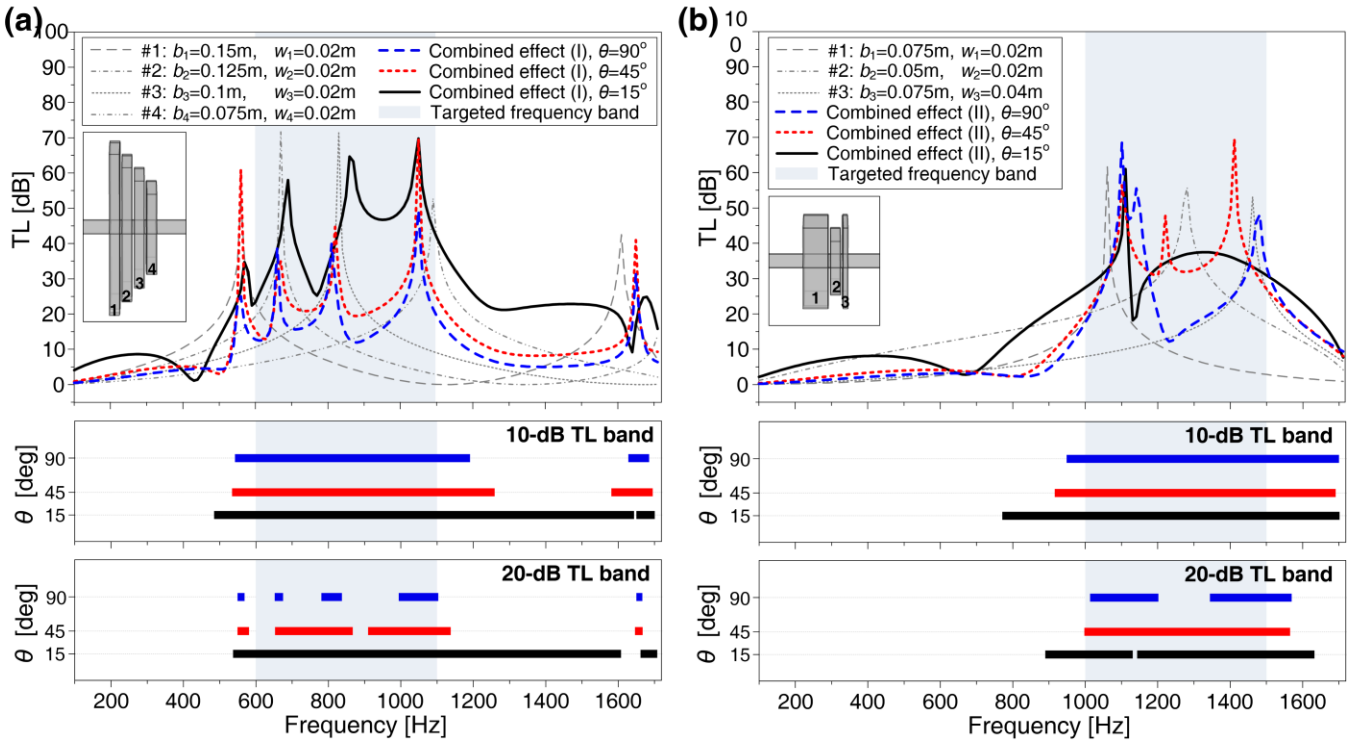

Figure 10. Two examples showing the programmability and modularization concepts based on combined effect of cascading multiple optimized silencer layers. The targeted frequency band (shaded) for (a) and (b) are [600, 1100] Hz and [1000, 1500] Hz, respectively. From the top to the bottom shows the TL curves, the 10-dB TL band, and the 20-dB TL band, respectively. For illustration purpose, TL curves of the constituent layers at the $\theta = 15^\circ$ configuration are provided; TL curves of the multi-layer silencer at the $\theta = 90^\circ$, $\theta = 45^\circ$, and $\theta = 15^\circ$ configurations are given.

If aiming at broadband TL, another set of five frequency subintervals are selected for programming the constituent layers: [200, 600] Hz, [600, 800] Hz, [800, 1000] Hz, [1000, 1200] Hz, and [1200, 1700] Hz. Table 1 and Figure 11 show that each frequency subinterval can be achieved by an optimized layer. By connecting these four layers in series, greatly enhanced broadband sound attenuation can be achieved. The 10-dB TL is obtained from 226 Hz to 1650 Hz, and the 20-dB TL also extends from 470 Hz to 1600 Hz. Comparing it with the case studied in Figure 3(b), which consists of four identical layers ($b = 0.1$ m and $w = 0.02$ m), the improvement is significant. Figure 11 also reveals that the TL peak frequencies of the multi-layer silencer largely agree with the TL peaks of the constituent layers. Around these peaks, namely, 510 Hz, 670 Hz, 840 Hz, 1070 Hz, and 1460 Hz, the sound attenuation is dominated by the corresponding constituent layer. Due to strong impedance mismatch, the sound wave can hardly be transmitted through the silencer. This is illustrated through the SPL surfaces in Figure 12, where the dominated layers are denoted by arrows.

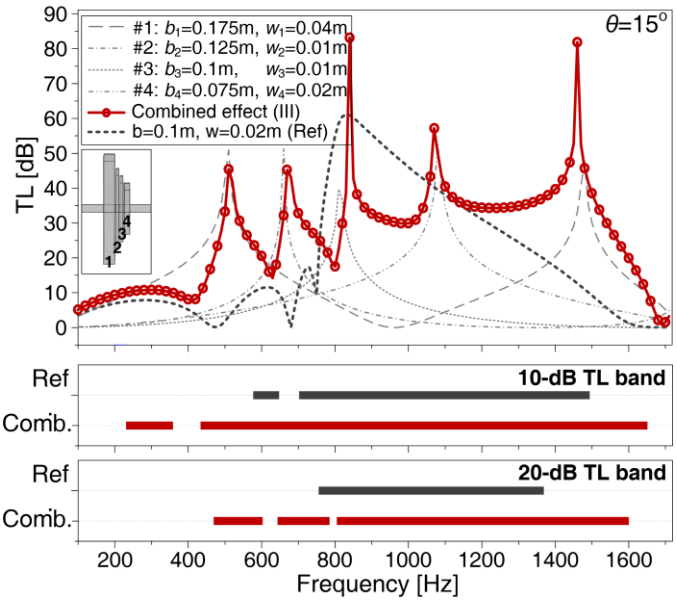

Figure 11. The third example showing broadband sound attenuation via programming the constituent silencer layers. From the top to the bottom shows the TL curves, the 10-dB TL band, and the 20-dB TL band, respectively. For illustration purpose, TL curves of the constituent layers are provided. All curves and band are based on the $\theta = 15^{\circ}$ configuration.

Table 1. The targeted frequency subintervals and the corresponding optimized layers in the third example

Targeted frequency subitervals	Optimized layer geometries	TL peak of the optimized layer
[200, 600] Hz	$b = 0.175$ m, $w = 0.04$ m	510 Hz
[1200, 1700] Hz		1480 Hz
[600, 800] Hz	$b = 0.125$ m, $w = 0.01$ m	660 Hz
[800, 1000] Hz	$b = 0.1$ m, $w = 0.01$ m	810 Hz
[1000, 1200] Hz	$b = 0.075$m, $w = 0.02$ m	1080 Hz

The above three examples well demonstrate the programmability of the modular origami silencer design. Owing to the excellent extensibility of the modular origami, without re-designing the whole silencer but just by programming and replacing the constituent layers, we are able to achieve (*i*) effective sound attenuation at the user-prescribed frequency bands (Examples 1 and 2) ; (*ii*) improved attenuation level (Examples 1~3); and (*iii*) broadband sound attenuation (Example 3). It is also worth pointing out that there can be more than one way to program the layers to meet specific objectives. Merits and demerits usually come together for one programmed configuration, and weighting the tradeoff is necessary in practical applications.

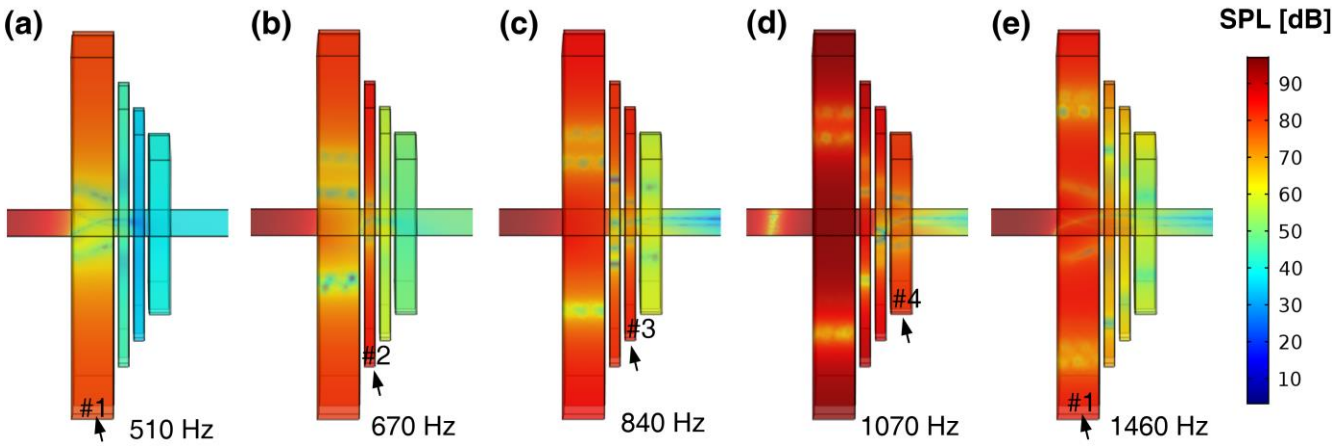

Figure 12. Sound pressure level (SPL) surfaces (side view) of the broadband multi-layer silencer (the third example, Figure 11) at the TL peak frequencies. (a) 5410 Hz, (b) 670 Hz, (c) 840 Hz, (d) 1070 Hz, and (e) 1460 Hz. The dominated layers are indicated by arrows.

6. Discussions and conclusions

Through a combined theoretical, numerical, and experimental investigation, this paper shows a novel concept for silencer design based on the modular origami concept. The new ideas explored in this research aims at offering an alternative method by which some existing bottlenecking problems in sound attenuation devices may be overcome, e.g., the lack of structural reconfigurabilty, acoustic tunability, and design flexibility that hamper the silencer adaptability to different working scenarios. Here the new reconfigurable origami silencer indeed provides promising resolutions to these problems in several aspects: origami folding can effectively alter the silencer configuration based on a single DoF mechanism and therefore allow the effective tuning of the attenuation bandwidth; modular origami's great extensibility offers the appealing programmability to silencer design such that performance adjustment can be achieved via replacing the constituent chamber layers. Through FE simulations and proof-of-concept experiments, this unconventional approach is proved to be feasible and effective in achieving these properties.

Note that as a proof-of-concept research, only one particular type of modular origami is investigated in this paper. Yet the modular origami design is limitless, and the corresponding changes of geometry will also impose positive or negative effects on the acoustic properties, which call for further examinations. For example, the four 'tiles' of the modular origami, i.e., the four chambers of a silencer layer, are identical in this study. By breaking the symmetries among the four chambers (Figure 13(a)), extra TL band may be generated and can be used for achieving broadband attenuation [38]. Besides, the

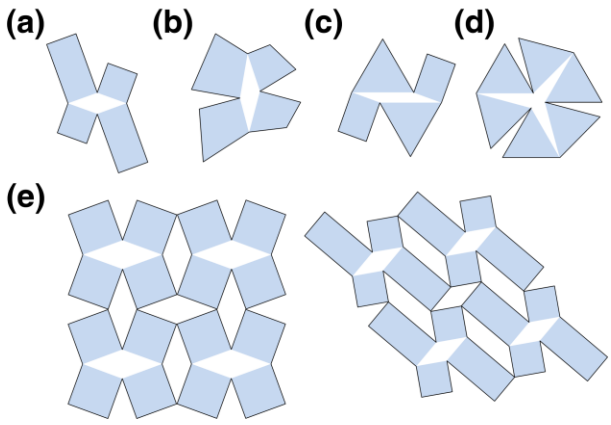

Figure 13. Various designs of modular origami units and modular origami meta-surfaces.

'tiles' are not necessary to be rectangular or square, they can change to irregular quadrilateral (Figure 13(b)) or triangle (Figure 13(c)); the folding mechanism can be changed from 4R linkage to 6R linkage such that six chambers would connect with the duct (Figure 13 (d)) [36]. Investigating their effects on acoustic properties would be interesting and would provide new design ideas. On the other hand, in addition to cascading different compatible layer in series, modular origami also possesses extensibility in plane. By repeating the basic cells in 2D, modular origami surface can be constructed (Figure 13(e)). They can be used as acoustic meta-surface with particular properties and functionalities. For example, a modular origami window with tunable air ventilation capability as well as tunable sound insulation performance can be expected [34]. It is worth mentioning that, by taking advantages of the interactions among periodically distributed ducts, a 2D modular origami meta-surface could be possible to exhibit other interesting and complex phenomena beyond our findings on a single unit. This is also an important future research direction to be built upon the methods and results reported in this paper.

Overall, in this research the scale-free folding kinematics of the modular origami and the duct acoustics are synergistically combined together to yield a reconfigurable origami silencer with acoustic tunability and programmability. By pointing out the rich design possibilities and the numerous potential applications, this research attempts to open a new avenue for the design and optimization of acoustic devices.

Acknowledgement. The authors would like to thank the undergraduate students Mr. Chun-Leung Cheung, Mr. Ka-Wai Tam, Ms. Tsz-Kwan Fung, Ph.D. candidate Mr. Xiaoqi Zhang and Mr. Tuo Liu from the Hong Kong Polytechnic University for their help in experiments.

References

[1] Munjal M L 2014 *Acoustics of Ducts and Mufflers* (Chichester, West Sussex, United Kingdom: John Wiley & Sons)

[2] Yu X and Cheng L 2015 Duct noise attenuation using reactive silencer with various internal configurations *J. Sound Vib.* **335** 229–44

[3] Lee J W and Jang G-W 2012 Topology design of reactive mufflers for enhancing their acoustic attenuation performance and flow characteristics simultaneously *Int. J. Numer. Methods Eng.* **91** 552–70

[4] Howard C Q and Craig R A 2014 An adaptive quarter-wave tube that uses the sliding-Goertzel algorithm for estimation of phase *Appl. Acoust.* **78** 92–7

[5] Yu X, Lu Z, Cheng L and Cui F 2017 Vibroacoustic modeling of an acoustic resonator tuned by dielectric elastomer membrane with voltage control *J. Sound Vib.* **387** 114–26

[6] Yu X, Lu Z, Cui F, Cheng L and Cui Y 2017 Tunable acoustic metamaterial with an array of resonators actuated by dielectric elastomer *Extrem. Mech. Lett.* **12** 37–40

[7] Dudte L H, Vouga E, Tachi T and Mahadevan L 2016 Programming curvature using origami tessellations *Nat. Mater.* **15** 583–8

[8] Fang H, Li S, Ji H and Wang K W 2016 Uncovering the deformation mechanisms of origami metamaterials by introducing generic degree-4 vertices *Phys. Rev. E* **94** 043002

[9] Overvelde J T B, Weaver J C, Hoberman C and Bertoldi K 2017 Rational design of reconfigurable prismatic architected materials *Nature* **541** 347–52

[10] Silverberg J L, Evans A A, McLeod L, Hayward R C, Hull T, Santangelo C D and Cohen I 2014 Using origami design principles to fold reprogrammable mechanical metamaterials *Science (80-.).* **345** 647–50

[11] Boatti E, Vasios N and Bertoldi K 2017 Origami Metamaterials for Tunable Thermal Expansion *Adv. Mater.* **1700360** 1700360

[12] Li S and Wang K W 2015 Fluidic origami with embedded pressure dependent multi-stability: a plant inspired innovation *J. R. Soc. Interface* **12** 20150639

[13] Silverberg J L, Na J, Evans A A, Liu B, Hull T C, Santangelo C D, Lang R J, Hayward R C and Cohen I 2015 Origami structures with a critical transition to bistability arising from hidden degrees of freedom *Nat. Mater.* **14** 389–93

[14] Waitukaitis S, Menaut R, Chen B G and van Hecke M 2015 Origami Multistability: From Single Vertices to Metasheets *Phys. Rev. Lett.* **114** 055503

[15] Fang H, Li S and Wang K W 2016 Self-locking degree-4 vertex origami structures *Proc. R. Soc. A Math. Phys. Eng. Sci.* **472** 20160682

[16] Li S, Fang H and Wang K W 2016 Recoverable and programmable collapse from folding pressurized origami cellular solids *Phys. Rev. Lett.* **117** 114301

[17] Felton S, Tolley M, Demaine E, Rus D and Wood R 2014 A method for building self-folding machines *Science (80-.).* **345** 644–6

[18] Fang H, Zhang Y and Wang K W 2017 Origami-Based Earthworm-Like Locomotion Robots *Bioinspir. Biomim.* **12** 065003

[19] Onal C D, Wood R J and Rus D 2013 An origami-inspired approach to worm robots *IEEE/ASME Trans. Mechatronics* **18** 430–8

[20] Filipov E T, Tachi T and Paulino G H 2015 Origami tubes assembled into stiff, yet reconfigurable structures and metamaterials *Proc. Natl. Acad. Sci.* **112** 12321–6

[21] Schenk M, Viquerat A D, Seffen K a. and Guest S D 2014 Review of Inflatable Booms for Deployable Space Structures: Packing and Rigidization *J. Spacecr. Rockets* **51** 762–78

[22] Rogers J, Huang Y, Schmidt O G and Gracias D H 2016 Origami MEMS and NEMS *MRS Bull.* **41** 123–9

[23] Lebée A 2015 From folds to structures, a review *Int. J. Sp. Struct.* **30** 55–74

[24] Fang H, Chu S-C A, Xia Y and Wang K W 2018 Programmable Self-Locking Origami Mechanical Metamaterials *Adv. Mater.* **30** 1706311

[25] Schenk M and Guest S D 2013 Geometry of Miura-folded metamaterials *Proc. Natl. Acad. Sci.* **110** 3276–81

[26] Liu X, Georgakopoulos S V and Tentzeris M 2015 A Novel Mode and Frequency Reconfigurable Origami Quadrifilar Helical Antenna *IEEE 16th Annual IEEE Wireless and Microwave Technology Conference (WAMICON)* (Cocoa Beach, FL) pp 13–5

[27] Fuchi K, Tang J, Member S, Crowgey B, Member S, Diaz A R, Rothwell E J and Ouedraogo R O 2012 Origami Tunable Frequency Selective Surfaces *IEEE Antennas Wirel. Propag. Lett.* **11** 473–5

[28] Harne R L and Lynd D T 2016 Origami acoustics: using principles of folding structural acoustics for simple and large focusing of sound energy *Smart Mater. Struct.* **25** 085031

[29] Zou C and Harne R L 2017 Folding Star-Shaped Acoustic Tranducers for Real-Time Guidence of Radiated Acoustic Waves *Proceedings of the ASME 2017 International Design Engineering Technical Conferences and Computers and Information in Engineering Conference* pp 1–7

[30] Babaee S, Overvelde J T B, Chen E R, Tournat V and Bertoldi K 2016 Reconfigurable origami-inspired acoustic waveguides *Sci. Adv.* **2** e1601019–e1601019

[31] Ishida S, Morimura H and Hagiwara I 2015 Sound-Insulating Performance of Origami-Based Sandwich Trusscore Panels *Origami 6: II. Technology, Art, Education* pp 431–8

[32] Thota M and Wang K W 2017 Reconfigurable origami sonic barriers with tunable bandgaps for traffic noise mitigation *J. Appl. Phys.* **122** 154901

[33] Thota M, Li S and Wang K W 2017 Lattice reconfiguration and phononic band-gap adaptation via origami folding *Phys. Rev. B* **95** 064307

[34] Yu X, Lu Z, Cheng L and Cui F 2017 On the sound insulation of acoustic metasurface using a sub-structuring approach *J. Sound Vib.* **401** 190–203

[35] Kim S H and Lee S H 2014 Air transparent soundproof window *AIP Adv.* **4** 117123

[36] Yang Y and Zhong Y 2017 Geometry of Modular Origami Metamaterials *Proceedings of the ASME 2017 International Design Engineering Technical Conferences and Computers and Information in Engineering Conference* pp DETC2017-67547

[37] Overvelde J T B, Jong T A De, Shevchenko Y, Becerra S A, Whitesides G M, Weaver J C, Hoberman C and Bertoldi K 2016 A three-dimensional actuated origami-inspired transformable metamaterial with multiple degrees of freedom *Nat. Commun.* **7** 10929

[38] Yu X, Tong Y, Pan J and Cheng L 2015 Sub-chamber optimization for silencer design *J. Sound Vib.* **351** 57–67

[39] Seo S-H and Kim Y-H 2005 Silencer design by using array resonators for low-frequency band noise reduction *J. Acoust. Soc. Am.* **118** 2332–8

[40] Tang S K 2012 Narrow sidebranch arrays for low frequency duct noise control *J. Acoust. Soc. Am.* **132** 3086–97

[41] Choy Y 2003 *Sound induced vibration and duct noise control* (The Hong Kong Polytechnic University)

[42] Hua X and Herrin D W 2013 Practical Considerations when using the Two-Load Method to Determine the Transmission Loss of Mufflers and Silencers *SAE Int. J. Passeng. Cars - Mech. Syst.* **6** 2013-01-1881

[43] To C W S and Doige A G 1979 A transient testing technique for the determination of matrix parameters of acoustic systems, II: Experimental procedures and results *J. Sound Vib.* **62** 223–33

[44] Lung T Y and Doige A G 1983 A time-averaging transient testing method for acoustic properties of piping systems and mufflers with flow *J. Acoust. Soc. Am.* **73** 867–76

[45] Bies D A, Hansen C H and Harward C W 2018 *Engineering Noise Controls* (Boca Raton, FL, USA: CRC Press)

[46] De Lima K F, Lenzi A and Barbieri R 2011 The study of reactive silencers by shape and parametric optimization techniques *Appl. Acoust.* **72** 142–50

[47] Lee T, Leok M and McClamroch N H 2009 Topology optimization of muffler internal partitions for improving acoustical attenuation performance *Int. J. Numer. Methods Eng.* **80** 455–77

[48] Chiu M C and Chang Y C 2008 Numerical studies on venting system with multi-chamber perforated mufflers by GA optimization *Appl. Acoust.* **69** 1017–37